Space Surveillance with Star Trackers. Part II: Orbit Estimation*

Ossama Abdelkhalik†, Daniele Mortari‡, and John L. Junkins§
Texas A&M University, College Station, Texas 77843-3141

Abstract

The problem of estimating the orbit of a space object using observed star tracker measurements, is addressed. Star trackers can provide azimuth and elevation measurements of a space object which are used to estimate the orbit of the object, assuming that the orbital and attitude motion models are known. The system observability is investigated. Both, batched least square and Kalman filter techniques, are implemented. Results show that the orbit parameters of the observed object can be estimated if the measurements time span is in the order of 20% of the orbital period.

1 Introduction

The ability to know precisely where a space object is orbiting the Earth is critical to mission planners for reaching science objectives as well as avoiding catastrophic collisions with other space objects or space debris. Currently, tracking information is provided by a number of facilities around the world including NASA's Satellite Laser Ranging (SLR) stations, the U.S. Air Force Space Surveillance Network, the U.S. High Accuracy Network Determination System (HANDS), the U.S. Navy Interferometer Fence, the Russian Space Surveillance System, the French Doppler Orbitography and Radio Position Integrated by Satellite system, as well as the U.S. Global Positioning

*Paper AAS 06-232 of the 16th AAS/AIAA Space Flight Mechanics Meeting, January 22-26, 2006, Tampa, Florida.

†Postdoctoral research associate, Department of Aerospace Engineering, 620C H.R. Bright Building, Texas A&M University, College Station, TX 77843-3141, Tel. (979) 458-0550, omar@tamu.edu

‡Associate Professor, Department of Aerospace Engineering, 611C H.R. Bright Building, Texas A&M University, College Station, TX 77843-3141, Tel. (979) 845-0734, Fax (979) 845-6051, mortari@tamu.edu

§Distinguish Professor, Department of Aerospace Engineering, 722B H.R. Bright Building, Texas A&M University, College Station, TX 77843-3141, Tel. (979) 845-3912, Fax (979) 845-6051, junkins@tamu.edu

System. The SLR stations provide some of the most accurate data that is often used to define "truth" orbits; however, its use is primarily limited to those space objects equipped with retro-reflectors.

Star trackers are the most accurate attitude sensors on board satellites. The main use is to accurately evaluate the spacecraft orientation with respect to the Earth Centered Inertial (ECI) reference frame, where usually the star catalog are provided. This is done by taking advantage from the invariance of the inter-star angles with respect to rotation and translation. However, due to the Sun reflectivity flying satellites can also be observed. Because of this, and because of the recent space threats increase, the idea of using the existing star trackers sensors to perform Space Surveillance, has been recently proposed and here investigated.

This paper proposes a novel method for estimating the orbit of a space object using star tracker measurements. Wide field-of-view star trackers along with a modified version of the "Pyramid" star identification algorithm[1] - "Pyramid-II" - provide angular measurements for the position of a space object in the field of view. "Pyramid-II" uses all the star-like objects appearing in the sensor field of view. Objects that are identified as belonging to the star catalog are then used for precision attitude estimation. As for the other star-like observations (unidentified space objects), which up to now have been simply discarded by standard star trackers data processing software, they are treated as regular stars, evaluating azimuth and elevation angles in the satellite's body frame. These measurements collected over a time span can provide enough information to estimate the orbit of the space object, assuming the model for its motion is known.

State of the art star trackers are today capable of taking measurements at frequencies approaching 100 Hz, hence, producing extremely dense short-arc in situ surveillance data of space objects within their field of view.

Since only azimuth and elevation angles are measured, the observability of the system is first investigated to check the possibility of estimating the system states from these measurements. Results of the observability investigation shows the possibility of estimating the space object given a minimum of time span for the measurements. Two methods are used for estimation, a *batched least square differential correction* and an *iterated Kalman filter* approaches.

In the following sections, the observability of the system is first investigated to check the possibility of estimating the system states from the measurements. For estimation purposes, the model of the system is here introduced and an analytical expression for the Jacobian matrix is derived. The Gaussian Least Squares Differential Correction (GLSDC) technique is implemented and results are presented.

2 Observability Investigation

In this section, the system observability is investigated to see whether the states of the system are independently observable from the measurements or not. For a linear system, this can be done by calculating the observability matrix and checking if it can be inverted or not. If it can be inverted, then all the states are observable from the measurements of the system [2]. For a nonlinear system, however, it is not that straight forward. The Newtonian gravitational attraction model is nonlinear. Even, if we assume small relative distance between the two spacecraft and use Hills equations as a model for the relative motion, the states equations are linear but the measurement is a nonlinear function of the states. Two cases will be considered to check the observability, the Hills equations model and the Newtonian attraction model.

2.1 Observability of the Nonlinear Model

In this nonlinear model, the system states are the object orbital elements and the true anomaly at the first measurement. The measurements are a series of directions from the observing spacecraft to the object spacecraft. The observability of the state vector from the measurements can be investigated by perturbing each of the states and check the resulting perturbation in the measured quantity [3]. If a perturbation of each of the states results in independent perturbation responses in the measured quantity, then all the states can be estimated from the measured quantity.

Each of the orbital elements for the object orbit is perturbed. These perturbations result in a corresponding perturbation in the vector of object position relative to the observing spacecraft position. The relative position vector can be seen as two separate quantities, magnitude, and direction. We are only concerned about the direction because this is the quantity that we can measure.

As a case study, it is assumed that the two spacecraft are moving in the same orbit with small eccentricity of 0.005 and an altitude of 550 Km. The observed object A is leading the observing spacecraft B. Figures 1-5 show the perturbation in the relative position distance and direction due to states perturbations. The direction is measured w.r.t. an inertial fixed axis.

As can be seen from Fig. 1, positive perturbation in the true anomaly at epoch results in constant positive perturbation in the direction of the relative position vector, ψ_{AB}. A negative perturbation causes also a negative constant perturbation in ψ_{AB}. Eccentricity perturbation causes harmonic perturbation in ψ_{AB}, as shown in Fig 2. Positive and negative eccentricity perturbations can be distinguished from each other from the phase difference in the perturbed ψ_{AB}. Since eccentricity perturbations cause harmonic ψ_{AB} perturbations compared to a constant perturbation for the case of the true anomaly at epoch, then these two states can distinguished from each other

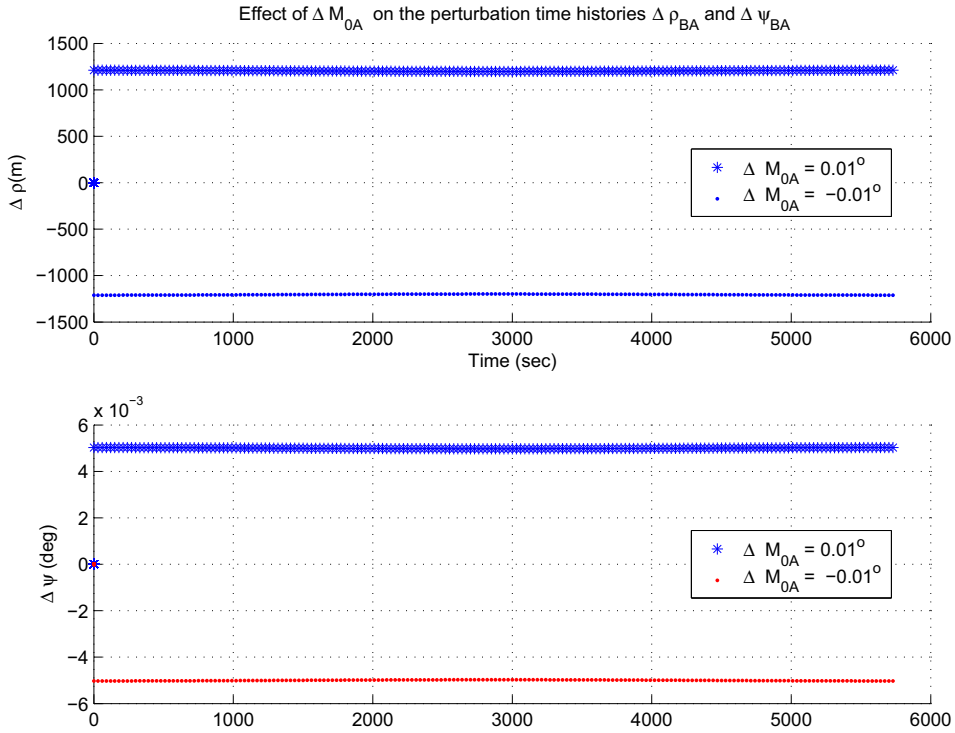

Figure 1: Perturbations of range and angle caused by perturbation of the mean anomaly at epoch

based on the measured ψ_{AB}. Considering Fig. 3, any perturbation in the semi major axis will cause the two spacecraft to orbit the Earth with different orbital period. This will result in ψ_{AB} changing as a ramp or even faster. Positive and negative perturbations in a, or equivalently in n, are distinguishable from each other based on the sign of the perturbed ψ_{AB}. Both are distinguishable from previous states because of the ramp nature of the ψ_{AB} response.

The orbit plane observability can be investigated geometrically as follows. First, consider the case of the two spacecraft are in the same plane. Then all the measured directions of the target spacecraft will be in the same plane. So, if all the measured directions are normal to the known observer plane normal vector, then the target spacecraft is in the observer plane. For the case of the two spacecraft are not in the same plane, consider the intersection point of the two orbits. The observer spacecraft orbit normal is known. The unit vector from the observer to the target at the intersection point is in the observer plane. So it is normal to the known observer plane normal vector. This means that the intersection points can be determined from the measurements: If the target direction is in the observer plane, then the target is at the intersection point at this time. Given the intersection points of the two orbits, and the plane of one of them, the plane of the second orbit cab be calculated geometrically.

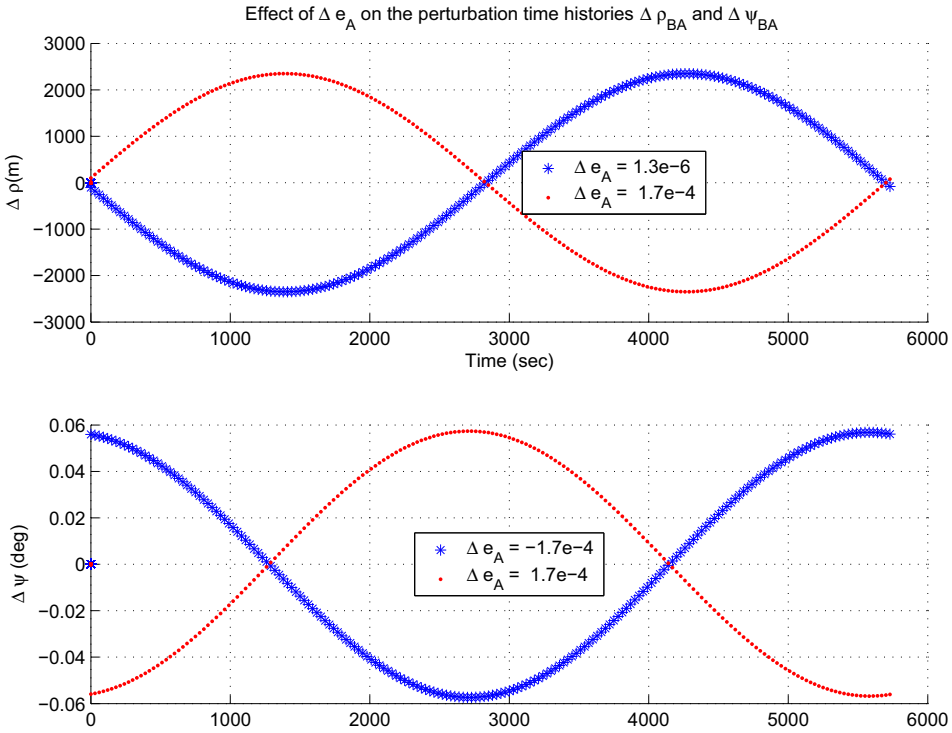

Figure 2: Range and angle variations due to eccentricity perturbation

From the above discussion, it can be concluded that all states can be estimated given a history of measurements. However, of importance is the duration of these measurements. Looking again at the previous figures, one can recognize that a short history of measurements, say 1000 seconds, may not tell whether the perturbed ψ_{AB} is, in this short period, a part of a ramp or a harmonic wave or even a constant with some noise added to it. It is concluded from that the measurements history should cover enough time to distinguish between different behaviors in the measured ψ_{AB}. This measurements period will depend on the two orbits of the two spacecrafts and some special cases may have special requirements. From the case studied above, one may conclude that a safe period of time is half the orbital period, or little less than that. As a demonstration for this concluded results; a GLSDC technique is used to estimate the states of a space object and the measurements are assumed ideal with no errors. Several cases are considered for different measurements duration period to see after how long measurements period can the estimator reach the true values. Consider the case of a LEO with eccentricity of 0.05, $h_p = 300$ Km, and inclination of 95°. Assume that the observing spacecraft is flying in an orbit with the same parameters but circular. Results are shown in Figs. 6-8. Figure 6 shows that the semi major length and eccentricity could not be estimated accurately after 20 minutes of time span. Even if we increase the number of measurements, 140 compared to 40 in the previous case, but still within the 20 minutes time span, we cannot estimate the true values, Fig. 7. However, if time span is increased to half of the orbital period, we get

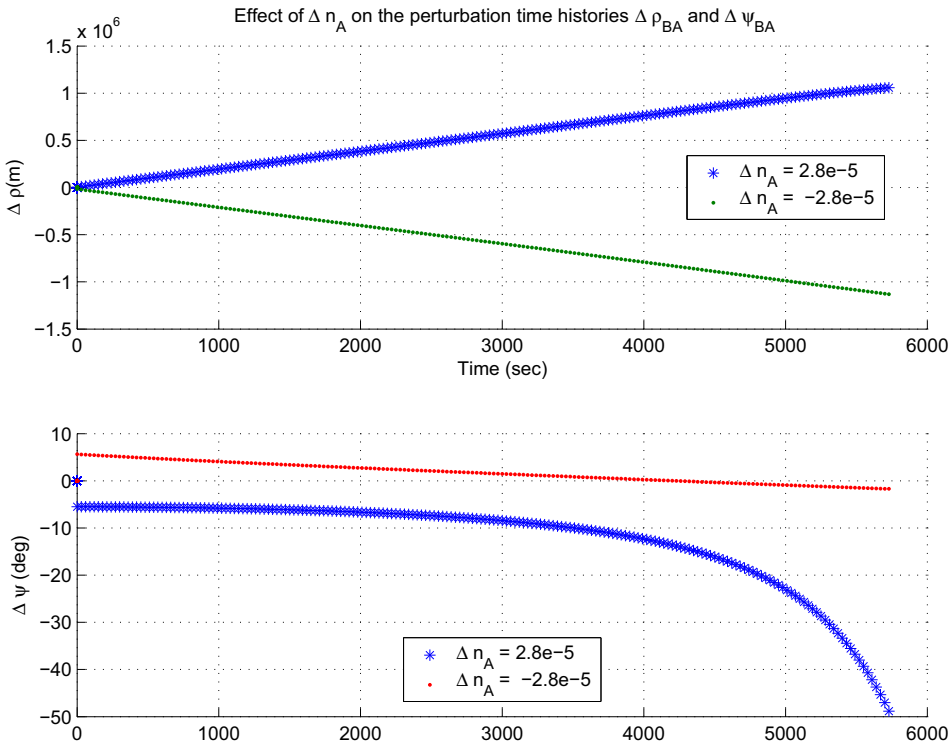

Figure 3: Perturbations of range and angle caused by perturbation of the semi-major axis

the true values as shown in Fig. 8. Reasonable measurements rate is still needed to accurately detect the harmonic behaviors in the measurements.

2.2 Observability of the Linear States Model

If the distance between the two spacecraft is small compared to the orbit size, and the orbit of the spacecraft is near circular, then the linear Hills equations [4] can be used to represent the relative motion of the two spacecraft

$$\begin{cases} f_x = \ddot{x} - 2\omega\dot{y} - 3\omega^2 x \\ f_y = \ddot{y} + 2\omega\dot{x} \\ f_z = \ddot{z} + \omega^2 z \end{cases} \tag{1}$$

where x, y, and z, are the three components of the object relative position w.r.t the observing spacecraft in the later's coordinate system. f_x, f_y, and f_z are the external forces applied to the object spacecraft. For the purpose of observability analysis, consider the solution of the above equations in the case of zero external forces [5]

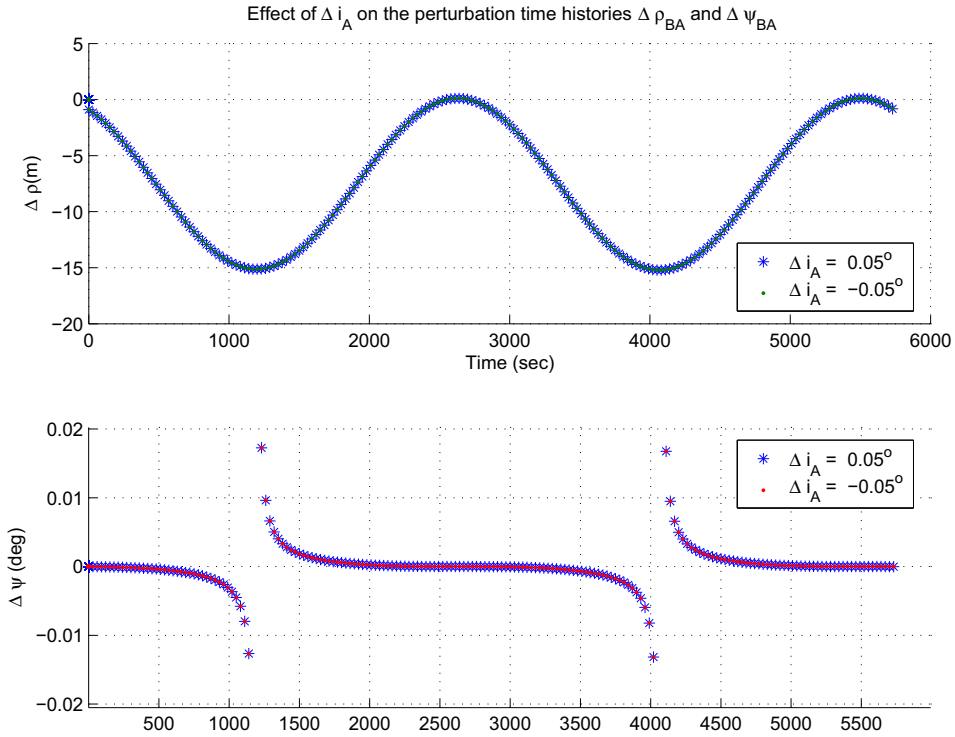

Figure 4: Perturbations of range and angle caused by perturbation of inclination

which can be written in a compact form as

$$\begin{cases} x(t) = f_1(x_0, \dot{x}_0, y_0, \dot{y}_0, t) \\ y(t) = f_2(x_0, \dot{x}_0, y_0, \dot{y}_0, t) \\ z(t) = f_3(z_0, \dot{z}_0, t) \end{cases} \tag{2}$$

The states that need to be estimated are the initial conditions: $x_0, \dot{x}_0, y_0, \dot{y}_0, z_0$, and $\dot{z}_0$. The measurement is the direction of the object spacecraft which can be considered as a unit vector in the direction of the object. So, a measurement $\mathbf{m}_k$ at time t_k is

$$\mathbf{m}_k = \frac{1}{\sqrt{f_{1k}^2 + f_{2k}^2 + f_{3k}^2}} \begin{Bmatrix} f_{1k} \\ f_{2k} \\ f_{3k} \end{Bmatrix} \tag{3}$$

where, f_{ik} is the function f_i evaluated at time t_k.

Given one measurement vector, Eq. (3) will give you three equations in six unknowns. Given two measurements, then we will have six equations in six unknowns. This set of nonlinear equations may have a single solution or multiple solutions. Additional measurements can be used to solve the ambiguities in the solution. So, from a mathematical point of view, This linear model is observable if we have two or more measurements.

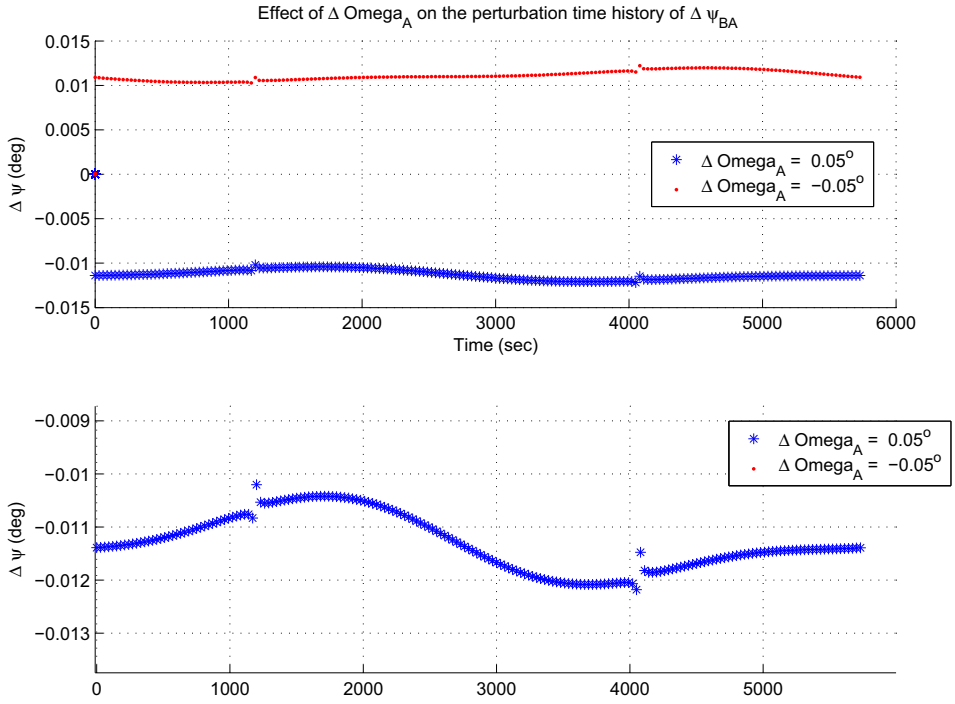

Figure 5: Perturbations of angle caused by perturbation of Ω_A

3 Gaussian Least Squares Differential Correction

The state variable vector $\mathbf{x}$ is selected to be

$$\mathbf{x} = \{\, a, \quad e, \quad i, \quad \omega, \quad \Omega, \quad \phi_0 \,\}^{\mathrm{T}} \tag{4}$$

where ϕ_0 is the true anomaly of the first measurement. The position of the object is $\mathbf{r}_o$. The position of the star tracker is $\mathbf{r}_s$. The position of the object with respect to the star tracker is $\mathbf{r}_{o/s}$. See Fig. 9 for geometry of the space surveillance problem. The model for m measurements,$\tilde{\mathbf{y}}_j$, is

$$\mathbf{y}_j = \mathbf{f}_j(\mathbf{x}), \quad j = 1 \ldots m \tag{5}$$

$$\mathbf{f} = \frac{\mathbf{r}_{o/s}}{\rho}, \qquad \rho = \|\mathbf{r}_{o/s}\| \tag{6}$$

So, Given a set of measurements $\tilde{\mathbf{y}}$, it is required to find the state vector $\mathbf{x}$. The motion of the object is assumed to follow a Keplarian orbit. The method of GLSDC is implemented.

The least squared error cost function

$$J = \frac{1}{2}\,\mathbf{e}^{\mathrm{T}}\, W\, \mathbf{e} = \frac{1}{2}\,[\,\tilde{\mathbf{y}} - \hat{\mathbf{y}}\,]^{\mathrm{T}}\, W\, [\,\tilde{\mathbf{y}} - \hat{\mathbf{y}}\,], \tag{7}$$

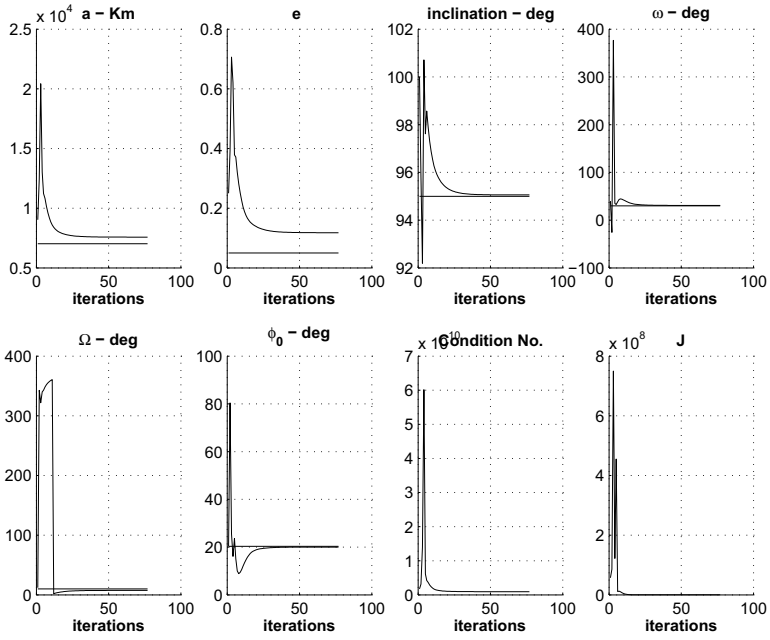

Figure 6: Time span = 20 min. No. of measurements = 40

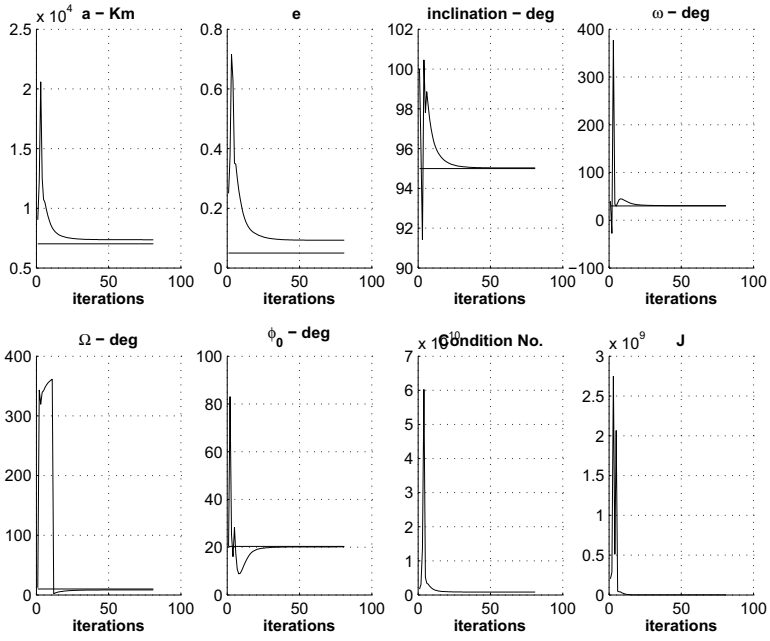

Figure 7: Time span = 20 min. No. of measurements = 140

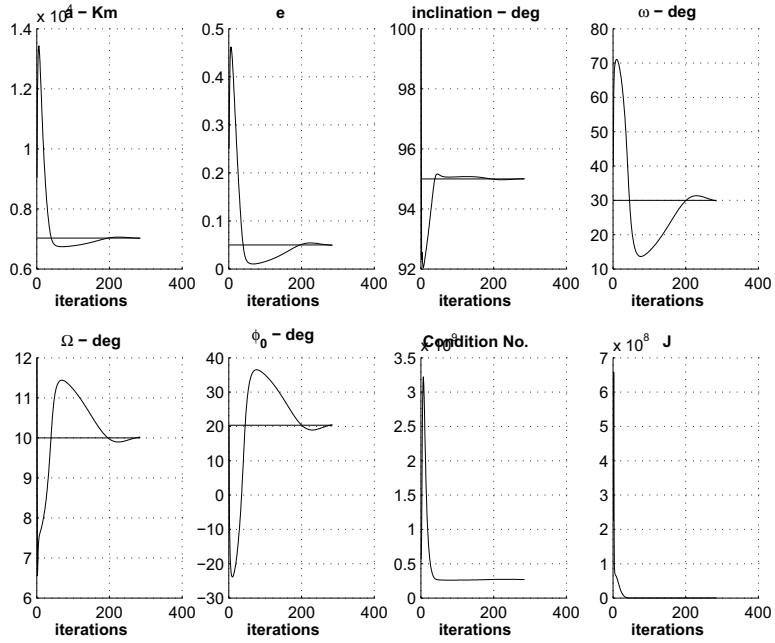

Figure 8: Time span = 50 min. No. of measurements = 140

is minimized by repeated state updates of the form

$$\Delta \mathbf{x} = (H^{\mathrm{T}}\, W\, H)^{-1}\, H^{\mathrm{T}}\, W\, [\, \widetilde{\mathbf{y}} - \mathbf{f}(\hat{\mathbf{x}}_i)\,] \tag{8}$$

where $\hat{\mathbf{x}}_i$ is the current estimate of the state, $H = \left.\dfrac{\partial \mathbf{f}}{\partial \mathbf{x}}\right|_{\mathbf{x}_i}$ is the Jacobian matrix, W is the weighting matrix, and $(H^{\mathrm{T}}\, W\, H)^{-1}$ is the auto-correlation matrix. If the weighting matrix is the inverse of the measurement variances, then the auto-correlation matrix becomes the error covariance.

4 Jacobian Matrix Derivation

The jacobian matrix, H, is by definition

$$H = \frac{\partial \mathbf{f}}{\partial \mathbf{x}} \tag{9}$$

Differentiating Eq. (6)

$$\rho \frac{\partial \mathbf{f}}{\partial \mathbf{x}} + \mathbf{f} \frac{\partial \rho}{\partial \mathbf{x}}^{\mathrm{T}} = \frac{\partial \mathbf{r}_{o/s}}{\partial \mathbf{x}} \tag{10}$$

where

$$\rho^2 = (\mathbf{r}_{o/s})^{\mathrm{T}} \mathbf{r}_{o/s} \tag{11}$$

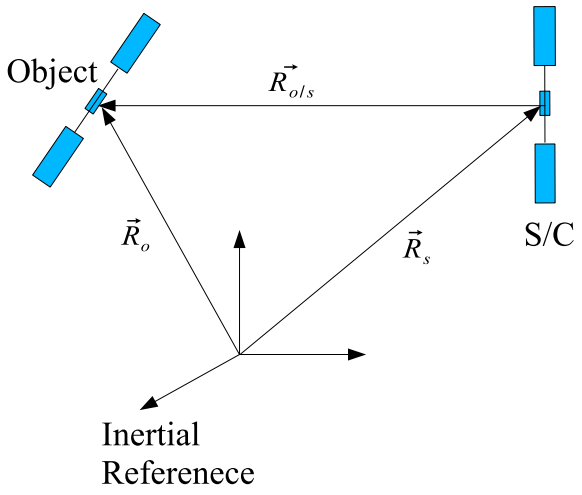

Figure 9: Geomtery for space surveillance

$$\frac{\partial \rho}{\partial \mathbf{x}} = \frac{1}{\rho} \left(\frac{\partial \mathbf{r}_{o/s}}{\partial \mathbf{x}} \right)^{\mathrm{T}} \mathbf{r}_{o/s} \tag{12}$$

So, to evaluate H, we need only to calculate $\dfrac{\partial \mathbf{r}_{o/s}}{\partial \mathbf{x}}$. In fact, since $\mathbf{r}_s$ is not a function of $\mathbf{x}$, then

$$\frac{\partial \mathbf{r}_{o/s}}{\partial \mathbf{x}} = \frac{\partial \mathbf{r}_o}{\partial \mathbf{x}} \tag{13}$$

The inertial position of the object at time t_j at which the measurement j was taken can be expressed as a function of the six orbital elements as follows [6]

$$(\mathbf{r}_o)_j = \xi(i, \Omega, \omega) \left\{ \begin{array}{c} a\,(\cos\psi_j - e) \\ a\sqrt{1-e^2}\,\sin\psi_j \\ 0 \end{array} \right\} \tag{14}$$

where

$$\xi(i, \Omega, \omega) = A_z^{\mathrm{T}}(\Omega)\, A_x^{\mathrm{T}}(i)\, A_z^{\mathrm{T}}(\omega) \tag{15}$$

and

$$A_z(\Omega/\omega) = \left[\begin{array}{ccc} \cos\Omega/\omega & \sin\Omega/\omega & 0 \\ -\sin\Omega/\omega & \cos\Omega/\omega & 0 \\ 0 & 0 & 1 \end{array} \right], \quad A_x(i) = \left[\begin{array}{ccc} 1 & 0 & 0 \\ 0 & \cos i & \sin i \\ 0 & -\sin i & \cos i \end{array} \right] \tag{16}$$

Differentiating Eq. (14) w.r.t. each of the six elements of $\mathbf{x}$

$$\frac{\partial (\mathbf{r}_o)_j}{\partial a} = \xi(i, \Omega, \omega) \left\{ \begin{array}{c} \cos\psi_j - e \\ \sqrt{1-e^2}\,\sin\psi_j \\ 0 \end{array} \right\} \tag{17}$$

$$\frac{\partial(\mathbf{r}_o)_j}{\partial e} = \xi(i,\Omega,\omega)\left\{\begin{array}{c} -a \\ -\dfrac{ae\sin\psi_j}{\sqrt{1-e^2}} \\ 0 \end{array}\right\} \tag{18}$$

$$\frac{\partial(\mathbf{r}_o)_j}{\partial i} = \frac{\partial\xi}{\partial i}\left\{\begin{array}{c} a\left(\cos\psi_j - e\right) \\ a\sqrt{1-e^2}\,\sin\psi_j \\ 0 \end{array}\right\} \tag{19}$$

$$\frac{\partial(\mathbf{r}_o)_j}{\partial \omega} = \frac{\partial\xi}{\partial \omega}\left\{\begin{array}{c} a\left(\cos\psi_j - e\right) \\ a\sqrt{1-e^2}\,\sin\psi_j \\ 0 \end{array}\right\} \tag{20}$$

$$\frac{\partial(\mathbf{r}_o)_j}{\partial \Omega} = \frac{\partial\xi}{\partial \Omega}\left\{\begin{array}{c} a\left(\cos\psi_j - e\right) \\ a\sqrt{1-e^2}\,\sin\psi_j \\ 0 \end{array}\right\} \tag{21}$$

where

$$\frac{\partial\xi}{\partial\Omega} = \frac{\partial A_z^{\mathrm{T}}(\Omega)}{\partial\Omega} A_x^{\mathrm{T}}(i)\, A_z^{\mathrm{T}}(\omega) \tag{22}$$

$$\frac{\partial\xi}{\partial\omega} = A_z^{\mathrm{T}}(\Omega)\, A_x^{\mathrm{T}}(i) \frac{\partial A_z^{\mathrm{T}}(\omega)}{\partial\omega} \tag{23}$$

$$\frac{\partial\xi}{\partial\Omega} = A_z^{\mathrm{T}}(\Omega) \frac{\partial A_x^{\mathrm{T}}(i)}{\partial\Omega} A_z^{\mathrm{T}}(\omega) \tag{24}$$

and

$$\frac{\partial A_z^{\mathrm{T}}(\omega)}{\partial\omega} = \left[\begin{array}{ccc} -\sin\omega & -\cos\omega & 0 \\ \cos\omega & -\sin\omega & 0 \\ 0 & 0 & 1 \end{array}\right], \quad \frac{\partial A_x^{\mathrm{T}}(i)}{\partial i} = \left[\begin{array}{ccc} 1 & 0 & 0 \\ 0 & -\sin i & -\cos i \\ 0 & \cos i & -\sin i \end{array}\right] \tag{25}$$

The derivative of $(\mathbf{r}_o)_j$ w.r.t. the true anomaly at the first measurement can be evaluated as follows

$$\frac{\partial(\mathbf{r}_o)_j}{\partial\phi_0} = \frac{\partial(\mathbf{r}_o)_j}{\partial\psi_j}\frac{\partial\psi_j}{\partial\psi_0}\frac{\partial\psi_0}{\partial\phi_0} \tag{26}$$

To calculate these derivatives, recall that

$$\tan\left(\frac{\psi_0}{2}\right) = \sqrt{\frac{1-e}{1+e}}\,\tan\left(\frac{\phi_0}{2}\right) \tag{27}$$

differentiating this equation, then

$$\frac{\partial\psi_0}{\partial\phi_0} = \sqrt{\frac{1-e}{1+e}}\,\frac{\sec^2\left(\dfrac{\phi_0}{2}\right)}{\sec^2\left(\dfrac{\psi_0}{2}\right)} \tag{28}$$

Recall also that

$$n(t_1 - t_p) = \psi_0 - e\,\sin\psi_0 \tag{29}$$

$$n(t_j - t_p) = \psi_j - e \sin \psi_j \tag{30}$$

Subtracting Eq. (29) from Eq. (30), then

$$\psi_j - e \sin \psi_j - \psi_0 + e \sin \psi_0 = n(t_j - t_1) \tag{31}$$

Differentiating Eq. (31) w.r.t. ψ_0 and taking into account that the difference in time between the two measurements, $t_j - t_1$, does not depend on ψ_0

$$\frac{\partial \psi_j}{\partial \psi_0} = \frac{1 - e \cos \psi_0}{1 - e \cos \psi_j} \tag{32}$$

Differentiating Eq. (14) w.r.t. ψ_j

$$\frac{\partial (\mathbf{r}_o)_j}{\partial \psi_j} = \xi(i, \Omega, \omega) \begin{Bmatrix} -a \sin \psi_j \\ a\sqrt{1 - e^2} \cos \psi_j \\ 0 \end{Bmatrix} \tag{33}$$

Combining Eqs. (32), (33), and (28), we obtain

$$\frac{\partial (\mathbf{r}_o)_j}{\partial \psi_0} = \xi(i, \Omega, \omega) \begin{Bmatrix} -a \sin \psi_j \\ a\sqrt{1 - e^2} \cos \psi_j \\ 0 \end{Bmatrix} \frac{1 - e \cos \psi_0}{1 - e \cos \psi_j} \sqrt{\frac{1 - e}{1 + e}} \frac{\sec^2 \left(\frac{\phi_0}{2} \right)}{\sec^2 \left(\frac{\psi_0}{2} \right)} \tag{34}$$

Equations (17-21) and Eq. (34) construct $\dfrac{\partial \mathbf{r}_o}{\partial \mathbf{x}}$. The last in turn is substituted into Eqs. (13), (12), and (10), to find H.

5 Results and Discussion

The above formulation is coded and the results show that this algorithm does not converge. The condition number for the matrix $(H^{\mathrm{T}}H)$ starts in the first iteration with a value in the order of 10^8 and rapidly increases as the number of iterations increase.

A small modification to the above formulation is done to try to get it to converge. The measurements vector is enhanced with an estimated value for the range of the object spacecraft. A virtual measurement vector is assumed to be the object inertial vector. This virtual measurements vector is calculated from the actual measurements vector as follows

$$(\mathbf{r}_o)_j = (\mathbf{r}_s)_j + (\mathbf{r}_{o/s})_j = (\mathbf{r}_s)_j + \rho_j \mathbf{y}_j \qquad j = 1, \ldots, m \tag{35}$$

The length ρ_j in Eq. (35) is calculated based on the current estimate for the state vector $\mathbf{x}$. This enhances the previous model with more information, the range of the

object spacecraft from the star tracker. However, this information is based on an estimate not actual measurements. The Jacobian matrix, H, is slightly modified. It is in this case, $H = \dfrac{\partial \mathbf{r}_o}{\partial \mathbf{x}}$. This modified algorithm converges.

It is possible to show that the above modified algorithm converges to the same solution of the original algorithm. The solution state vector $\hat{x}$ is the minimizing state vector for the cost function

$$J = \frac{1}{2}\,\mathbf{e}^{\mathrm{T}}\,W\,\mathbf{e} \tag{36}$$

where the residual error vector, $\mathbf{e}$, is the difference between the measurements vector and its model

$$\mathbf{e} = \tilde{\mathbf{y}} - \mathbf{f}(\hat{\mathbf{x}}) \tag{37}$$

The new measurement vector can be written as

$$\tilde{\mathbf{y}}' = \{\, \tilde{\mathbf{y}}^{\mathrm{T}} \quad r \,\}^{\mathrm{T}} \tag{38}$$

where $\hat{r}$ is an estimate for the range of the object spacecraft. The the new residual error vector is

$$\mathbf{e}' = \{\, \mathbf{e}^{\mathrm{T}} \quad 0 \,\}^{\mathrm{T}} \tag{39}$$

The new cost function is then

$$J' = \frac{1}{2}\,\mathbf{e}'^{\mathrm{T}}\,W\,\mathbf{e}' = \frac{1}{2}\mathbf{e}^{\mathrm{T}}\,W\,\mathbf{e} = J \tag{40}$$

So, the two algorithms actually search for the same minimum for the same cost function. The solution provided by this algorithm is described and analyzed through the discussion of the following figures. The figures below show the convergence history and the number of iterations required for convergence. The true values of the states are plotted as horizontal lines in figures.

The first case presented is a case with $2,000$ measurements, collected 5 times per second. This is about 7 minutes of spacecraft flight. The results are shown in Fig. 10. The results show convergence to the true values. This can lead to the conclusion that with more iterations, a good estimate can be achieved. The drawback is the running time; with this big number of measurements, $2,000$ measurements, the Jacobian matrix becomes very big.

As shown earlier in the observability investigation section, for better estimation results, the total time span of observations should be increased. So, the number of measurements is reduced to be only 70 and the time between measurements is increased to be 33 seconds. The measurements duration is then about 39 minutes of observations. This resulted in decreasing the running time significantly since the number of measurements is much smaller. The results of this case are shown in Fig. 11 and Fig. 12. Figure 11 shows a good convergence to the true values. The inclination of the orbit is almost exactly correct. Other states converge to a steady state

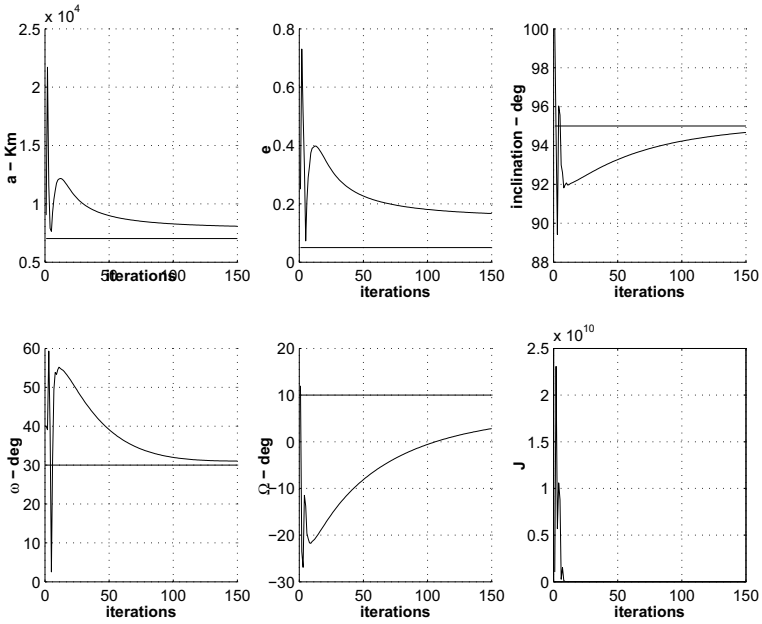

Figure 10: GLSDC, measurements collected 5 times/second

value that is biased from the true value. For the purpose of analysis, the same case is run again but this time with ideal measurements. The only error is the initial guess. Results of this run are shown in Fig. 12. All states almost converges very close to the true values. It can be concluded that the biased estimate of the states is due to the model of measurements errors.

To check how small the time span can be, the case of 15 minutes of measurements duration is considered. Several runs are performed and the results showed instability in the solution depending on the number of measurements and on the measurements errors. As a result, with only 15 minutes of measurements, sometimes we can get a convergence and some times not. One example of a case that converged is shown in Fig. 13. If we increase the time of measurements duration to 20 minutes which is about 20% of the true orbital period, the algorithm will converge independent from the number of measurements.

Two cases are plotted for a number of measurements of 40 and 100. All converged to a close value to the true states. The condition number history for the matrix $(H^{\mathrm{T}} W H)$ is plotted. It is always below the order of 10^{10}. As the number of measurements increase, a better accuracy is achieved. This can be figured out by comparing Fig. 14 and Fig. 15. The error in the measurements is assumed to be Gaussian with a maximum of 1 km in each coordinate direction.

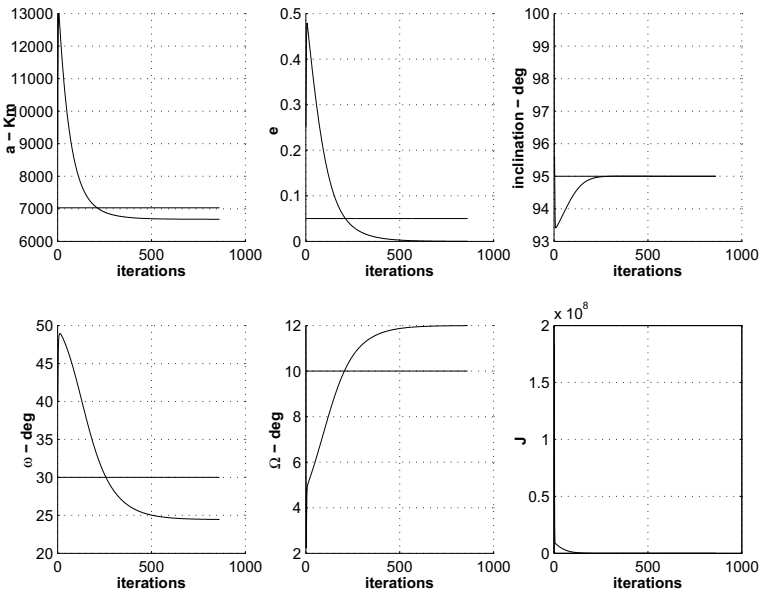

Figure 11: Measurements collected 2 times/min. for 39 minutes

6 Iterated Kalman Filter

In this section the extended Kalman filter technique [7] is implemented for estimation. The state vector is chosen to be the initial position and velocity vectors. The truth model used is

$$\ddot{\mathbf{r}} = -\frac{\mu}{\| \mathbf{r}(t)^3 \|} \mathbf{r}(t) + \mathbf{w}(t) \tag{41}$$

$\mathbf{w}(t)$ is the process noise, which is assumed to be zero. The Extended Kalman Filter converges much faster than the least square technique implemented in the previous section. The extended Kalman filter is used to process data forward with guessed initial conditions, and then process the data backward. Initial conditions for the backward pass are the final states of the forward pass. Each iteration consists of a forward and a backward pass. Figure 16 shows the estimated initial position and velocity using the iterated Kalman filter.

7 Conclusions

The orbit of a space target can be estimated using the measurements of a star tracker. An important factor is how long is the time span in which the measurements are taken. Initial analysis performed in this study shows that the orbit parameters can be estimated if the measurements cover a time span of the order of 10% to 20% of the orbital period, depending on the target orbit. The target orbit plane however can be estimated in much less time span, which is in the order of 5% to 10% of the orbital

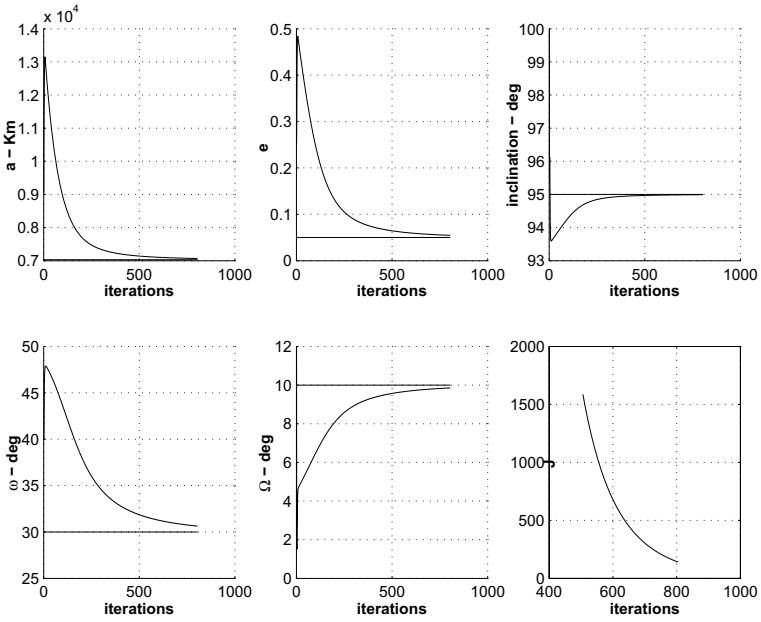

Figure 12: Measurements collected 2 times/min. for 39 min., initial error only

period.

References

[1] Mortari, D., Samaan, M. A., Bruccoleri, C., and Junkins, J. L., "The Pyramid Star Identification Technique," *Navigation*, Vol. 51, No. 3, Fall 2004, pp. 171–183.

[2] Ogata, K., *Modern Control Engineering*, Prentice Hall of India, New Delhi, India, 2nd ed., 1991.

[3] Psiaki, M. L., "Autonomous Orbit Determination for Two Spacecraft from Relative Position Measurements," *Journal of Guidance, Control, and Dynamics*, Vol. 22, No. 2, March-April 1999.

[4] Clohessy, W. and Wiltshire, R., "Terminal Guidance System for Satellite Rendezvous," *Journal of the Aerospace Sciences*, September 1960, pp. 653–658.

[5] Vallado, D. A., *Fundamental of Astrodynamics and Applications*, STL, 2001.

[6] Sidi, M. J., *Spacecraft Dynamics and Control*, 1997.

[7] Crassidis, J. L. and Junkins, J. L., *Optimal Estimation of Dynamic Systems*, CHAPMAN&HALL/CRC, 2004.

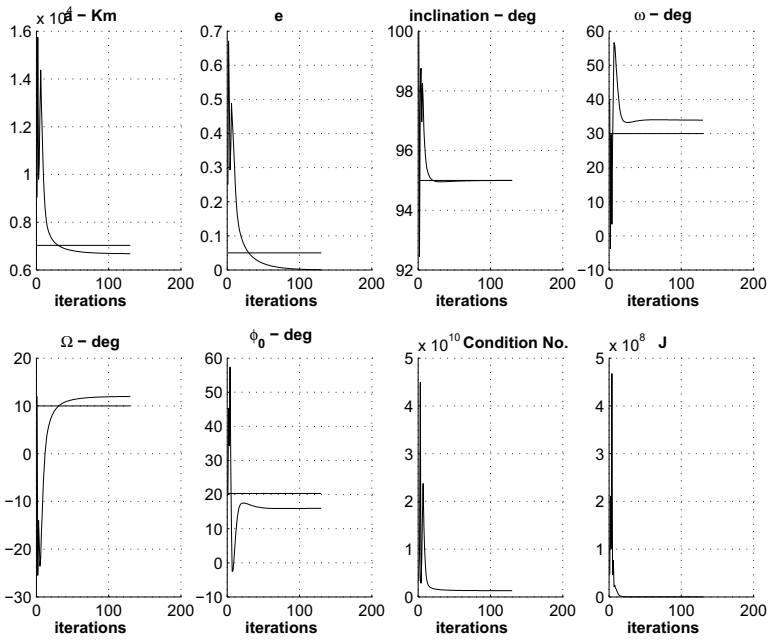

Figure 13: Measurements duration = 15 min. No. of measurements = 40

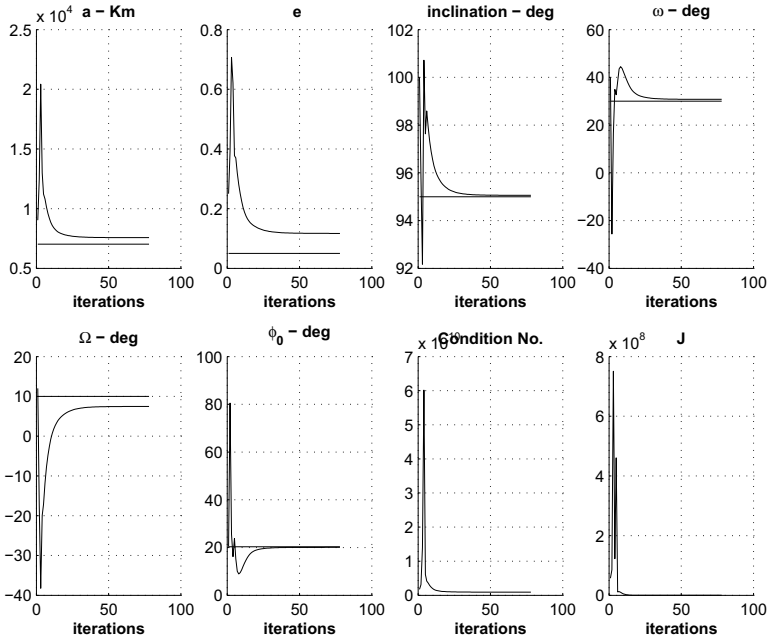

Figure 14: Measurements duration = 20 min. No. of measurements = 40

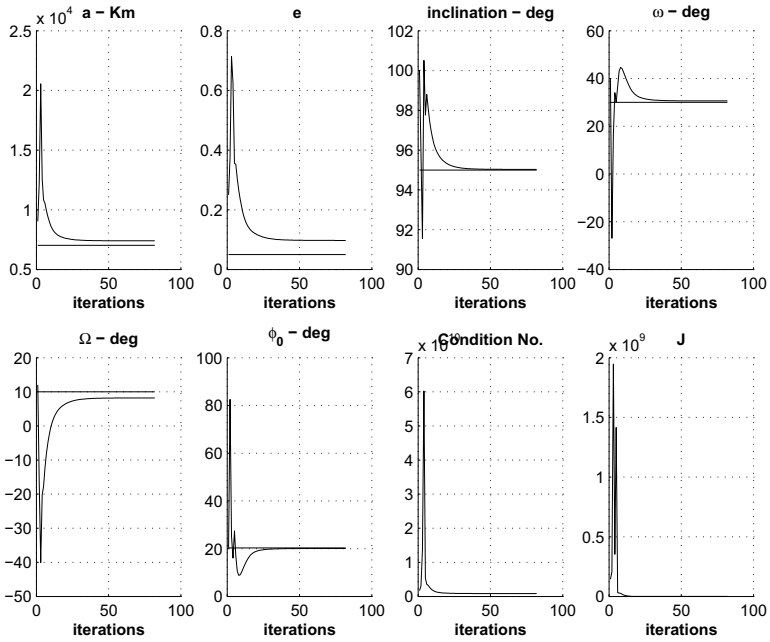

Figure 15: Measurements duration = 20 min. No. of measurements = 100

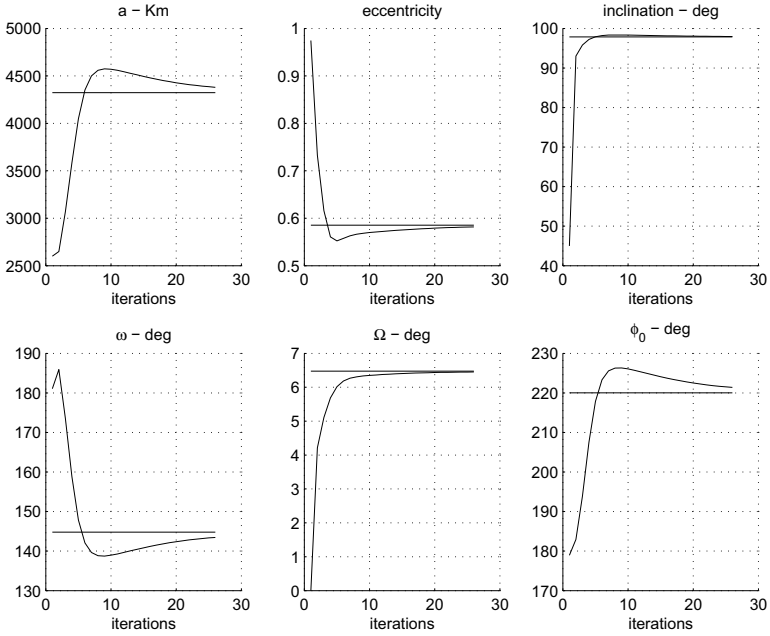

Figure 16: Iterated Kalman filter, time span=10 min, No. of measurements=11